Adaptation of a k-epsilon Model to a Cartesian Grid Based Methodology

Stephen M. Ruffin and Jae-Doo Lee

***Abstract* -** Despite the high cost of memory and CPU time required to resolve the boundary layer, a viscous unstructured grid solver has many advantages over a structured grid solver such as the convenience in automated grid generation and vortex capturing by solution adaption. In present study, an unstructured Cartesian grid solver is developed on the basis of the existing viscous solver, NASCART-GT. Instead of a cut-cell approach, an immersed boundary approach is applied with ghost cell boundary condition, which can be easily applied to a moving grid solver. The standard k-ε model by Launder and Spalding is employed for the turbulence modeling, and a new wall function approach is devised for the unstructured Cartesian grid solver. In this study, the methodology is validated and the efficiency of the developed boundary condition is tested in 2-D flow field around a flat plate, NACA0012 airfoil, and axisymmetric hemispheroid.

Keywords – Cartesian Grid, Computational Fluid Dynamics, Turbulence Model

NOMENCLATURE

c_p	=	specific heat
C_p	=	pressure coefficient
η	=	local coordinate normal to wall
I_t	=	turbulent intensity
μ_l	=	molecular viscosity
μ_t	=	eddy viscosity
$\boldsymbol{n}$	=	normal vector of surface panel
r	=	recovery factor
Pr	=	Prandtl number

I. INTRODUCTION

UNSTRUCTURED grid computational fluid dynamics (CFD) methods can employ automated grid generation for complex geometries (see [1] and [2]) and solution adaption for vortex capturing far more readily than structured grid methods. In spite of these advantages of the unstructured grid topology over the structured grid, until recently it could not be used for a viscous flow calculation due to the high cost of memory and CPU time to resolve the boundary layer. As high performance parallel computer systems have become more recently available, the unstructured grid solvers have been very popular even in the calculation of viscous and turbulent flow.

Many unstructured grid solvers use pyramid or prism type grid topology, in which the cells are body-fitted and it is easy to apply conservative integration for finite volume method. However, the numerical solution of the equations of fluid dynamics is simplified and the truncation error is reduced, if the discretization is performed in a Cartesian coordinate system. Many flow simulations involve complex geometries with curved and planar boundaries oblique to the grid. For an accurate simulation, the computational domain of Cartesian grid solver should include arbitrary cut cell near the solid [3]. A common problem with cut cell is the creation of very small cells. This leads to problems with stiffness of the equations and non-physical fluctuations of flow variables near the body. In case of time-dependent simulations, it limits the time step and influences the stability. Researchers have dealt with this in a number of ways, including hybrid grid [4] merged cell approach [5],[6] and embedded cell method [7].

The hybrid grid topology employs the body-fitted structured grid near wall combined with Cartesian grid away from body. Using a structured grid near wall, however, means an often laborious grid generation process for complex configurations.

The merged cell approach uses a Cartesian grid for all cells except those which are intersected by the boundary in Fig. 1. The boundary cells are truncated and merged into a nearest flow cell so that they conform to the shape of the boundary surface. Since the flow properties at the merged cell center are integrated from the wall boundary and flow cells, the state vector is always conservative. However, it generally entails a considerable increase in complexity, since fluxes between diagonally adjacent cells must also be calculated, and the computational molecule for merged boundary cells become different to that used for the standard cells. Since the merged cell center is not aligned with other flow cells, the order of accuracy in spatial discretization is limited during integration of flow cells contacting the merged cell.

Manuscript received June 2, 2009.
S.M. Ruffin is with the School of Aerospace Engineering at the Georgia Institute of Technology, Atlanta, GA 30332-0150 USA. Phone: 404-894-8200; Fax: 404-894-2760; Email: Stephen.ruffin@ae.gatech.edu
J.D.Lee is with Samsung Heavy Industries, Co. LTD., Daejeon, 305-380, Korea

The earlier version of NASCART-GT used an embedded boundary method. In this approach (described in [7]), wall boundary conditions were enforced by extrapolating to cut cell centers. The embedded boundary method removes the surface cells from the finite volume formulation and extrapolates flow properties on the boundary cell center from a reference point. However, it requires some relocation of the cell center to the centroid of the cut cells as shown in Fig. 2.

The immersed boundary method using ghost cells was first introduced by Forrer and Jeltsch [8] for Cartesian grid. The boundary cell is not truncated and maintains cubic shape. As shown in Fig. 2, the boundary cell center is not shifted to the cut-cell center and maintains at the centroid of non-cut cell independent of boundary shape. Dadone [9] successfully solved the 2D and 3D Euler equation for an unstructured Cartesian grid using the ghost-cell immersed boundary method. He considered solid walls as boundaries immersed in the flow field and enforced boundary conditions at ghost cell centers located inside the body in a position close to the wall. It solved the problem of the misalignment of cell centers. It also eliminated the requirement of finding cell centroids thereby saving computer memory.

To date, most unstructured Cartesian grid techniques have been developed to solve the Euler equations. Excluding the hybrid grid solver, there has been relatively little research for the full Navier-Stokes or RANS equations. Furthermore, no viscous modeling using an immersed cell approach has been reported yet. It is quite challenging and has never done before to apply wall function approach to immersed Cartesian grid. The difficulty lies in the inability to acquire smooth variation of y^+ in the desired range due to the non-body-fitted cells near the solid wall. Applying the conventional wall function wall boundary condition on the immersed Cartesian cells near the wall would result in a large magnitude of non-physical fluctuations of the flow properties, thereby, cause instability of the computation. The wall function boundary condition developed in this work yields stable and reasonable solution within the accuracy of the turbulence model. The grid efficiency is also improved with respect to the conventional method by extending the first cell center from the wall boundary up to $y^+ \approx 300$.

II. NUMERICAL FLOW SOLVER

NASCART-GT (Numerical Aerodynamic Simulation via CARTesian Grid Technique) is a finite volume, compressible, unsteady, three-dimensional Cartesian grid solver of the RANS (Reynolds Averaged Navier-Stokes) equation set, which assumes calorically perfect gas. The molecular viscosity is calculated from Sutherland's law. The RANS equations are solved using Roe's approximate Riemann solvers coupled with a MUSCL scheme for inviscid fluxes and traditional finite differencing of the viscous terms. The primitive variables at the hanging node are interpolated using 2nd order pseudo-Laplacian averaging scheme. For turbulent flow simulation, the standard k-ε model by Launder and Spalding [10] is employed. The time integration is performed using a Hancock two-stage scheme which is second order accurate in time. To ensure the positivity of turbulent quantities, a turbulent limiter is applied derived from the asymptotic analysis of k and ε equations. Solution adaption is performed at user-specified iteration numbers based on divergence, vorticity, turbulent kinetic energy and dissipation rate. For more detail, see [11]. The following sections explain boundary conditions in detail.

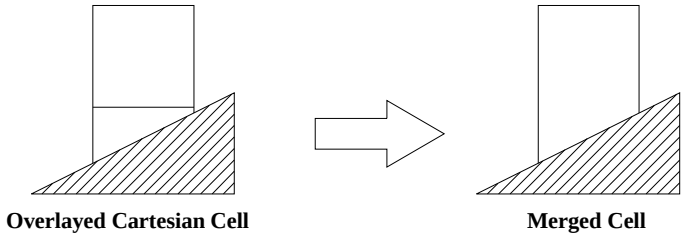

Fig. 1. Illustration of merged cell approach.

For outflow and inflow boundaries, characteristic boundary condition or simple extrapolation is applied to specify Riemann invariants. For turbulent flow calculation, the turbulent kinetic energy and dissipation rate are assumed to be known at the inlet boundary from the prescribed turbulence intensity and the turbulent viscosity. A value for the ratio of freestream turbulent viscosity to laminar viscosity is also specified, such that

$$k_\infty = \left(I_t V_\infty\right)^2 \tag{1}$$

$$\mu_{t,\infty} = C_1 \mu_\infty \tag{2}$$

The resultant freestream turbulent dissipation is obtained from turbulent viscosity closure. I_t is generally set to 0.01 for external flows. Improper value of C_1 may result in slow convergence. In NASCART-GT, it is set to 0.1. Limiting the values of k and ε of the flow cell to the freestream values after each time step, helps prevent unphysical transient solution [12]. At the outflow boundary, k and ε are extrapolated according to the characteristic boundary condition.

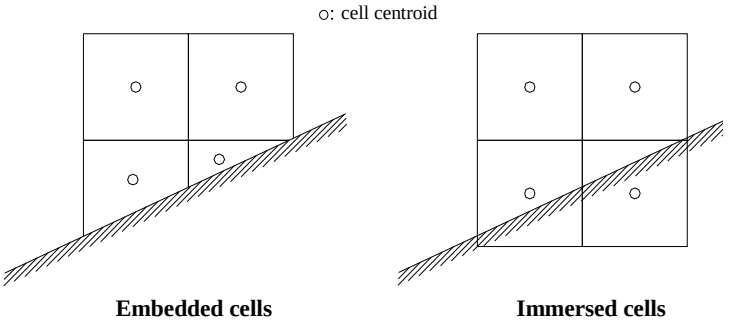

Fig. 2. Comparison of embedded and immersed cells.

Instead of directly specifying wall boundary conditions on a wall, NASCART-GT enforces primitive variables on the ghost cells such as 15 and 16 in Fig. 3, which act as wall boundaries. The state vector of cells intersected by the solid wall (called boundary cells, for example, 11, 12 and 14 in Fig. 3) are found

using time integration as the same manner with flow cells. The point B and D represent the reference points of cell 16 and 15

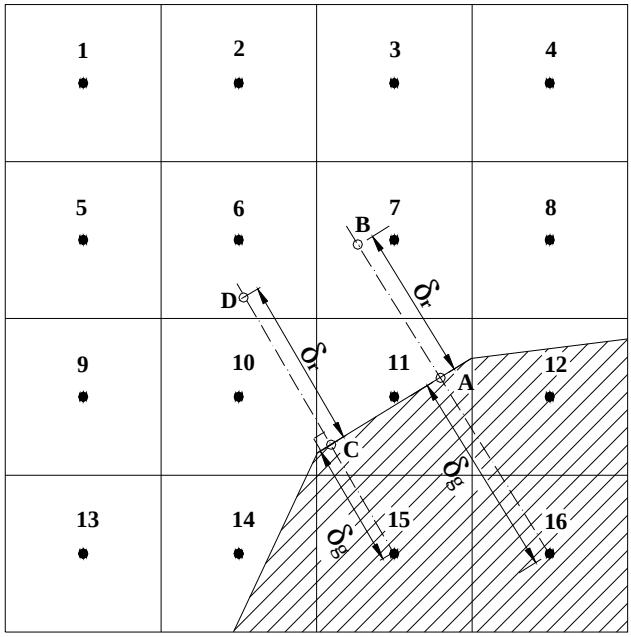

Fig. 3. Example configuration of wall boundary treatment. Boundary cells: 11, 12, 14. Ghost Cells: 15, 16. Remainder of cells are flow cells.

respectively. The location of reference point is determined as following. First, find the closest point on a body panel from the ghost cell center, i.e. point A or C. Then, extend the line connecting the ghost cell center and the closest point on the wall panel to the extent of predetermined length, δ_r . In current study, δ_r is set to the length of boundary cell diagonal. The primitive variables at a reference point are interpolated from the primitive variables of the 3 closest neighbor cell centers using the linear least square interpolation. After finding primitive variables at the reference point, the variables at the ghost cell center are calculated using linear extrapolation.

For pressure, the condition $\partial p/\partial \eta = 0$ is satisfied by setting the pressures on the wall and the ghost cell center are identical to that at the reference point, i.e. $p_{ref} = p_w = p_g$, where the subscripts ref , w and g denote reference point, wall and ghost cell center, respectively. Adiabatic wall boundary condition is fulfilled when $\partial T/\partial \eta = 0$ is enforced as the same manner with the pressure boundary condition. To find the velocity components at the ghost cell center, the velocity at the reference point is transformed to get the tangential and normal velocities.

$$\boldsymbol{V}_{N,ref} = \left(\boldsymbol{V}_{ref} \cdot \boldsymbol{n}\right)\boldsymbol{n} \tag{3}$$

$$\boldsymbol{V}_{T,ref} = \boldsymbol{V}_{ref} - \boldsymbol{V}_{N,ref} \tag{4}$$

where the subscripts N and T represent normal and tangential components, respectively. Normal velocity on the wall should be zero in a non-permeable wall. Thus, linear extrapolation results in

$$\boldsymbol{V}_{N,g} = -\frac{\delta_g}{\delta_r}\boldsymbol{V}_{N,ref} \tag{5}$$

The next step is to define the tangential velocity and temperature at the ghost cell center using the law of the wall. NASCART-GT employs the Spalding's formulation, which yields a unified form valid for the log law layer and the viscous sublayer as well as the buffer layer. It is known that the Spalding's formulation shows excellent agreement with various experimental data even after, for $y^+ > 300$, the outer law commences [13].

$$y^+ = u^+ + e^{-\kappa B}\left[e^{\kappa u^+} - 1 - \kappa u^+ - \frac{\left(\kappa u^+\right)^2}{2} - \frac{\left(\kappa u^+\right)^3}{6}\right] \tag{6}$$

For the given temperature and tangential velocity at the reference point, the adiabatic wall temperature is calculated from the Crocco-Busemann equation.

$$T_w = T_{ref} + \frac{r}{2}\frac{V_{T,ref}^2}{c_p} \tag{7}$$

where r is the recovery factor known to be $\Pr^{1/3}$ in turbulent flows for air. c_p represents the specific heat. The wall density is obtained from the state law for calculated wall temperature and wall pressure that is equal to the reference point pressure. Then, the wall shear stress at the reference point can be calculated by solving Eq. (6) numerically, i.e. Newton's method.

The next step is to implement the computed wall shear stress into the governing equations. With coarse grid spacing near wall, incorrect velocity gradient and wall shear stress will be obtained when no-slip condition is applied. One approach to introducing the wall function corrected wall shear stress into the calculation of the viscous flux is to calculate the effective turbulent viscosity so that the discrete shear stress at the boundary cell face yields the correct value for the wall shear stress [14]. Unfortunately, this method may results in errors into the energy equation if a separate effective turbulent viscosity for the temperature is not used.

Instead of modifying turbulent viscosity, calculated shear stress by wall function can be directly imposed on the face near wall. Sondak and Pletcher [15] introduced a procedure to perform a transformation of the stresses for generalized coordinate system with body-fitted structured grid. He used the standard tensor transformation to get

$$\tau_{\alpha\beta} = \frac{\partial \xi_\alpha}{\partial x_i}\frac{\partial \xi_\beta}{\partial x_j}\tau_{ij} \tag{8}$$

where α and β represent the geodesic coordinate, and i and j the Cartesian coordinate. However, the above method needs a very complicated coordinate transformation, which would increase truncation error and emasculate the advantage of the Cartesian grid. To make the matters worse, non-physical fluctuations of primitive variables are induced when Sondak's method is combined with the staggered Cartesian grid. The fluctuations may result in fictitious separation and distort the whole solution. This is mainly caused by the opposite directional velocity of the cells whose center is located inside of the wall. The nonlinear velocity profile combined with sharp change in the distances from the cell center to the wall induces the non-physical fluctuations.

To solve previously stated problems, a new wall function boundary condition is devised in the present study. It is based on the idea that the modified tangential velocity satisfying discrete wall shear stress approximation would eliminate the use of the complicated coordinate transformation. This allows the computational cells near wall to remain in numerically linear region, thereby, the computation would be stable. The approach is described in the following.

The normal velocity is specified by the Eq. (5) to ensure zero normal velocity on the wall. Since the total wall shear stress near the wall is approximately constant, the wall shear stress at the ghost cell is set to be the same as that at the reference point. Assuming the total viscosity (the sum of molecular viscosity and eddy viscosity) of the ghost cell is identical to that of the reference point, the shear stress in the solver is approximated as

$$\tau_w \approx \left(\mu_{l,ref} + \mu_{t,ref}\right)\frac{\Delta V_T}{\Delta \eta} = \left(\mu_{l,ref} + \mu_{t,ref}\right)\frac{V_{T,ref} - V_{T,g}}{\delta_r - \delta_g} \quad (9)$$

Then, the tangential velocity of the ghost cell is

$$V_{T,g} \approx V_{T,ref} - \frac{\delta_r - \delta_g}{\mu_{l,ref} + \mu_{t,ref}}\tau_w \quad (10)$$

Applying linear tangential velocity at the ghost cells may result in non-physical mean velocity at boundary cells. However, this condition satisfies the required wall boundary conditions of zero normal flux and wall shear stress, and the flow cells outside of the boundary cells would have proper values. The pressure boundary condition is in the same manner with the laminar wall conditions. The temperature of the ghost cell follows the Crocco-Busemann relation from the reference point temperature and computed tangential velocity. This is based on the fact that the adiabatic wall temperature is constant along the normal ray near wall.

$$T_g = T_{ref} + \frac{r}{2}\frac{V_{T,ref}^2 - V_{T,g}^2}{c_p} \quad (11)$$

The density is obtained from the state law. The remaining step is to find the boundary conditions for turbulent properties, k and ε. The boundary conditions of k and ε have to satisfy the assumption of the Eq. (9). At the same time, the eddy viscosity should follow the designated profile, which is described in the [16].

$$\frac{\mu_t}{\mu_l} = \kappa e^{-\kappa B}\left[e^{\kappa u^+} - 1 - \kappa u^+ - \frac{\left(\kappa u^+\right)^2}{2}\right] \quad (12)$$

To fulfill these requirements, the boundary conditions for turbulent properties are imposed on the flow cells contacting the boundary cells, as well as the ghost cells and boundary cells. Fig. 3 shows the example of the flow cells (e.g. the cells 6~9, and 13), on which the turbulent boundary conditions are enforced. Assuming that the shear stress is constant near the wall, the turbulent kinetic energy at the cell center is equal to

$$k = \frac{u_\tau^2}{\sqrt{C_\mu}} \quad (13)$$

Given the eddy viscosity from the Eq. (12), the dissipation rate of the turbulence energy is set to satisfy the turbulent viscosity according to the Launder and Spalding's turbulence model.

$$\varepsilon = C_\mu \rho \frac{k^2}{\mu_t} \quad (14)$$

For boundary cells and ghost cells, the turbulent properties are specified using the reference point properties. The constant total viscosity condition along the ray yields to

$$\mu_t = \mu_{l,ref} + \mu_{t,ref} - \mu_l \quad (15)$$

The turbulent kinetic energy and dissipation rate are specified using the equations (13) and (14), respectively.

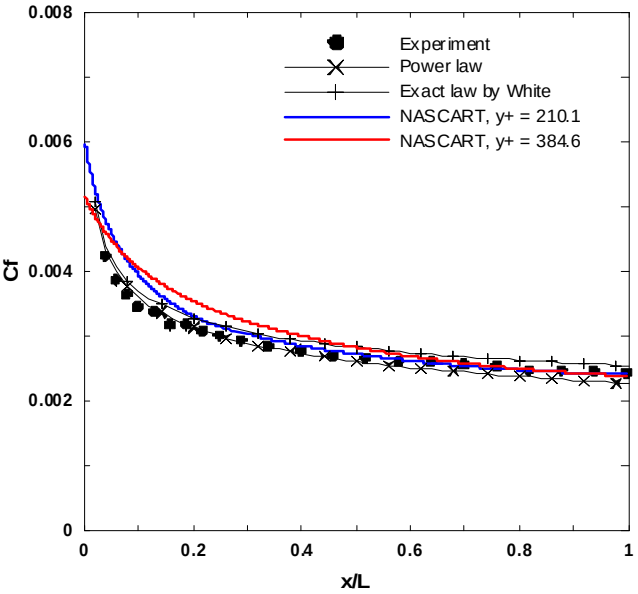

Figure 4. Computed C_f over turbulent flat plate.

Although applying a wall function is efficient, it may not be expected to identify the separation point as accurately as high grid resolution turbulence models (e.g. low Reynolds k-ε model and LES) can. Many researchers have shown that wall function approaches can be highly successful in the calculation of separated flow in high adverse-pressure-gradient regions such as shock-wave near a boundary layer [17], high speed cascade [18], and a step flow [19]. However, it is not easy to capture an exact separation point and may yield delayed separation with wall function approach in mild adverse-pressure-gradient regions, which is true for the developed wall function boundary condition as most of the wall function approaches. Further research may be required to find out how the developed approach works in a separated flow region.

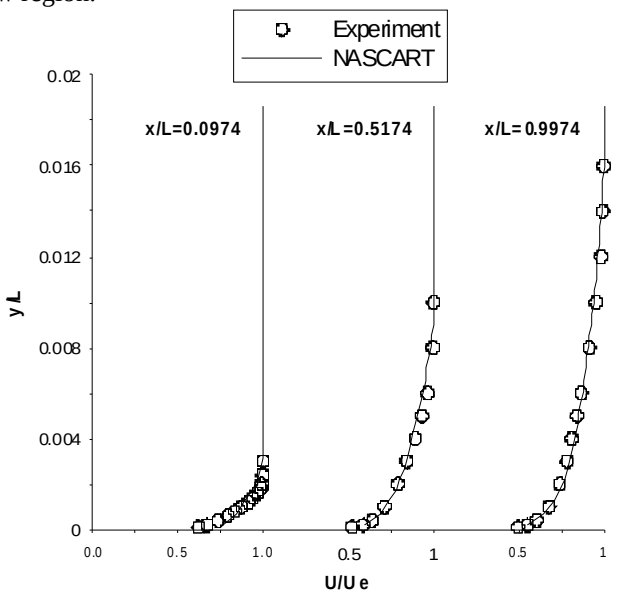

Fig. 5. Mean velocity profiles on turbulent flat plate.

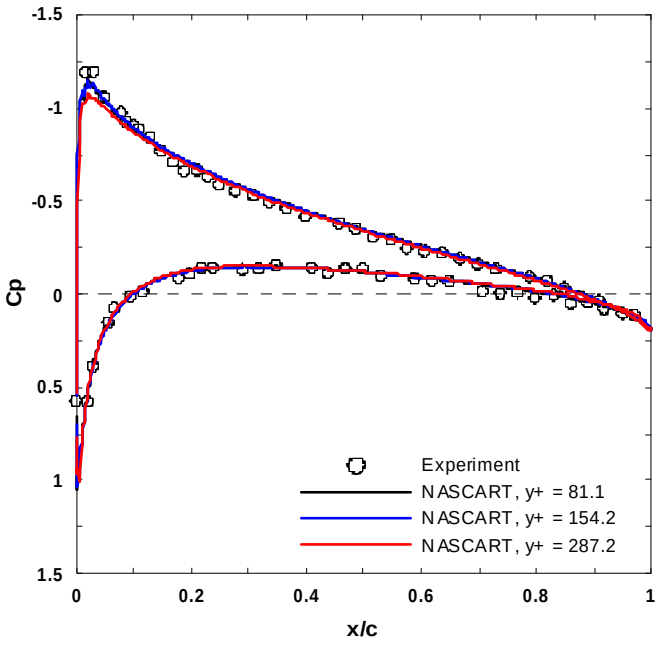

Fig. 6. Pressure coefficients with various cell sizes over turbulent NACA 0012 airfoil.

III. VALIDATIONS

The validation of the developed numerical approach is performed on the various 2-D viscous flows including turbulent flows over flat plate and NACA 0012 airfoil, and the axisymmetric turbulent flow over a hemispheroid. The results are compared with analytical solution or experimental data. All the results shown in this chapter are obtained using the 3rd order interpolation of the inviscid fluxes.

A. Flat Plate

A body-aligned Cartesian grid is generated to calculate turbulent flow over a two-dimensional flat plate. Inflow boundary is located ahead of the leading edge, and outflow boundary is on the trailing edge. On the inflow boundary, the characteristic boundary condition is enforced as usual. On the upper and outflow boundaries, however, the primitive variables are extrapolated instead of characteristic boundary condition to ensure the flow smoothly sweep out. The freestream Mach number is set to 0.2 to avoid incompressible limit of the solver.

The Reynolds number based on flat plate length is 1.0927×10^7, at which the skin friction and velocity profiles have been measured by Wieghardt [20]. The computational domain and root cell dimension are identical to the laminar calculation. However, the grid is finer than the laminar case such that the maximum grid refinement levels are 8 for coarse grid and 9 for fine grid. This results in the largest y^+ values of 384.6 and 210.1, respectively, based on the reference point, which are larger than the cell size requirement of most RANS solvers. The surface roughness parameter was not measured, either. A value of $B = 5.0$ was used in the law of the wall assuming smooth wall.

The computed skin friction is compared with the power law, exact law by White [13], and the experiments in Fig. 4. Aft of the mid-chord, the measured skin friction is between the power law and the exact law, which is well analyzed by NASCART. As shown in the picture, the skin friction changes rapidly near the leading edge. The inaccuracy of the computed skin friction near the leading edge might be caused by the insufficient local grid resolution. It is easily noted that the difference between the results of the computations and experiments near the leading edge is decreased as the y^+ decreases. It is expected that the computed skin friction will further approach to the experimental data with higher grid resolution. In spite of the small error near the leading edge caused by insufficient grid resolution, the solution with the coarse grid shows good agreement with the results of fine grid computation and experiment at the trailing edge.

Fig. 5 shows the comparison of computed with fine grid and measured mean velocity profile at various locations. It is observed that the calculated mean velocity profile and boundary layer thickness have good correlation with the measurements. Slight over-prediction of the boundary layer thickness from station 1 thru 4 is also induced by the insufficiently large cells, which smears out the high velocity gradient.

B. NACA 0021 Airfoil

Turbulent modeling is tested over a NACA0012 airfoil at a Mach number of 0.3, a chord Reynolds number of 1.86 million, and an incidence of 3.59 degrees. The computational boundaries are the same as the laminar calculation. The root grid dimension is 22×20 and 8, 9 and 10 levels of refinement are applied to get the maximum y^+ based on the reference point of 81.1 up to 287.2. The characteristic boundary conditions are applied on the inflow and outflow boundaries. A smooth wall is assumed to specify $B = 5.0$ for the law of the wall. The computed mean surface pressure coefficients are compared with AGARD experimental data [21] in Fig. 6, and very good correlations are observed even with very coarse grid of y^+=287.2.

For the quantitative analysis of the grid efficiency, the effects of the cell sizes on the accuracy and computational cost from the solutions of NACA 0012 airfoil flows are presented in Table 1. Errors are calculated based on the airfoil data [22] and the savings on the solutions of the RANS with the fine grid. There is little difference between computed lift coefficients for fine and medium grids whose errors are less than 0.2 %. Meanwhile the savings of computer memory and computation time are observed by over 48 % and 62 %, respectively. As mentioned before, conventional wall function approach requires small cells near wall to yield y^+<80 for proper turbulence modeling. This demonstrates the fact that the developed wall function approach has better grid efficiency and computational time than the conventional methods. Considering the coarse grid case, the accuracy is deteriorated just by 2.813 % while the computational time is improved by over 93 % with respect to the fine grid solution and over 81 % to the medium grid solution. It is, therefore, apparent that the implementation of coarse grid with the developed wall function method is practical and efficient approach in the overall prediction of the aerodynamic forces, yielding reasonable solution within the accuracy of the present turbulence model.

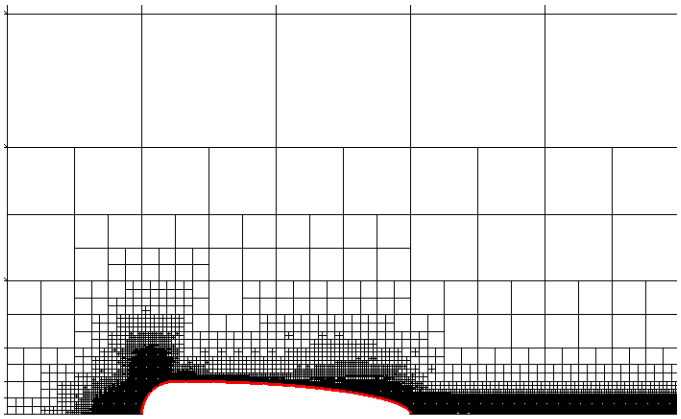

Fig. 7. Final grid configuration over axisymmetric hemispheroid.

C. Axisymmetric Hemispheroid

The turbulent boundary layer on the hemispheroid was measured by Ramaprian et al. [23] to provide validation data for computational development. The model configuration combines a hemispherical nose with a hemispheroidal rear. The experiments are performed at the Reynolds number (based on the length of the body) of 2.0×10^6. The nominal wind-tunnel velocity is 22.0 $m/\sec$ thereby $M_\infty \approx 0.063$. The computational Mach number is increased to avoid the incompressible limit of the code, and the computations are performed for axisymmetric flow. The velocity profile and skin friction are measured at 8 traverse stations, which are shown in the reference. The computational boundaries are 5 times body length ahead of and behind the hemispheroid, above and below the centerline. The root grid dimension is 28×24, and 8, 9, and 11 levels of refinement are applied. The freestream Mach number is increased to 0.3 to prevent poor conditioning of the compressible flow solver. The constant related to the roughness parameter is set to $B = 5.5$ according

Table 1. Effect of cell size on accuracy and computational cost for NACA 0012 airfoil calculations.

Grid density		Fine	Medium	Coarse
Accuracy	c_l	0.3584	0.3583	0.3489
	[+] Error (%)	0.1671	0.1950	2.813
Computer memory	No. of cells	72,520	37,672	20,176
	[++] Saving (%)	N/A	48.1	72.2
Computation time	* CPU time (hr)	44.7	16.9	3.1
	[++] Saving (%)	N/A	62.2	93.1

[+] Based on the airfoil data of $c_l = 0.3590$

[++] Based on the RANS fine grid calculation

∗ CPU time is obtained using Pentium IV 2.4 GHz PC

to the experiments. Fig. 7 shows the final grid configuration, in which the red line represents the wall boundary. The cells are refined near the leading edge and wake region where the large gradients of divergence and vorticity exist. The computed mean pressure distributions are shown in Fig. 8, compared with the experimental data. The pressures are measured at circumferential angles of 0 and 120 degrees. The difference between the measured pressures is very small, and the computational results show very good agreement with them even with $y^+ \approx 300$. In Fig. 9, calculated mean skin friction is compared with the experiment, in which the skin friction is measured at the circumferential angles of 0 and 180 degrees. Since the flow is axisymmetric, the difference between these two is considered as an experimental error. According to the reference paper, the estimated error of the instrument in the wall shear stress measurement is 5 %. It is, however, reported that a considerable uncertainty exists due to the deviation of the angle between the velocity vector and the probe axis. Therefore, the error of the measured skin friction is assumed to be 10 % that corresponds to the difference of skin friction coefficients at station 6. The results of NASCART are well correlated to the experiment within the estimated error with the exception of the first measurement station. At station 1, the computed skin friction is overestimated, which also has been observed by Sondak and Pletcher [10]. They computed the turbulent flow over the same hemispheroid using three turbulence models (Baldwin-Lomax algebraic model, Launder and Spalding $k-\varepsilon$ model, and Chien's low Reynolds number $k-\varepsilon$ model), and none of the models predicts the proper skin friction at station1. This discrepancy would be caused by the transition from laminar to turbulent flows in the experiment, which is not modeled in numerical analysis. This would explain the fact that the measured skin friction coefficient is lower than the computed values and that the computation over-predicts the tangential velocity at station 1 in the subsequent plot. The computed velocity distributions with fine grid are presented in Fig. 10, and the results compare reasonably well with the test data.

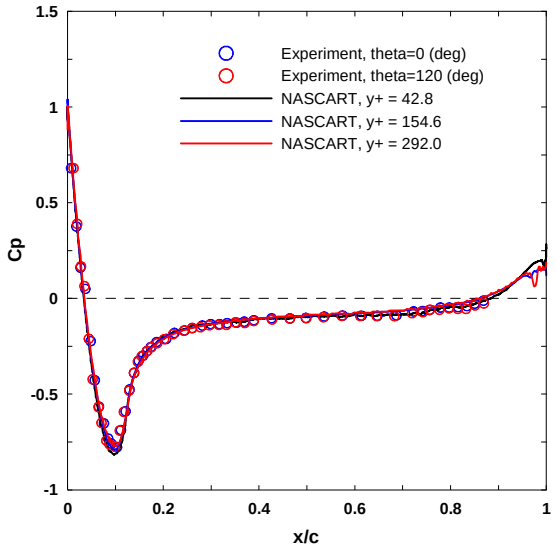

Fig. 8. Pressure coefficients with various cell sizes over hemispheroid.

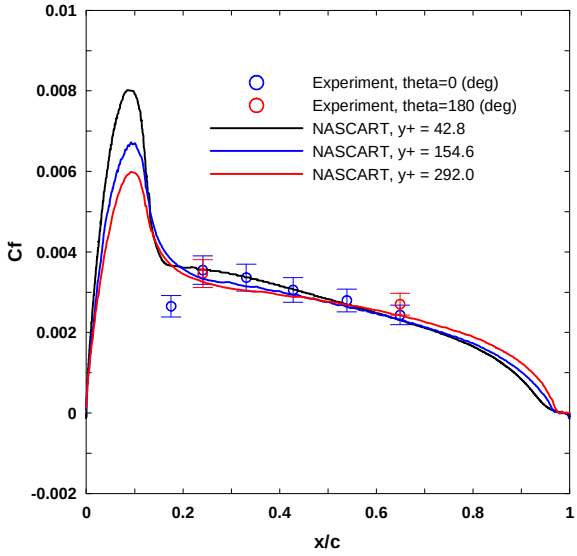

Fig. 9. Skin friction coefficients with various cell sizes over hemispheroid.

IV. CONCLUSIONS

In present study, new viscous wall boundary conditions are implemented into the existing unstructured Cartesian grid framework. A number of conclusions are shown below.

- The boundary cell centroids aligned with the flow cell centers make the numerical stencil orthogonal and reduce the error in the volume integration. The application of ghost cell approach also increases the accuracy by the use of conservative volume integration in the calculation of boundary cells just like in flow cell calculation instead of simple extrapolation of the flow properties. This yields an accurate prediction of skin friction and velocity profile in a boundary layer as well as the pressure.
- The new boundary condition is developed and successfully tested for an immersed Cartesian grid viscous solver. The developed wall function approach yields stable and reasonable solution within the accuracy of the turbulence model. The new approach removes the complicated coordinate transformation required in the conventional wall function approach.
- Unlike the conventional wall function approach, the developed method shows stable and reasonable solution with a relatively coarse grid system within the accuracy of the turbulence model. The use of a coarse grid with the developed wall function approach can reduce the computational memory and computation time.

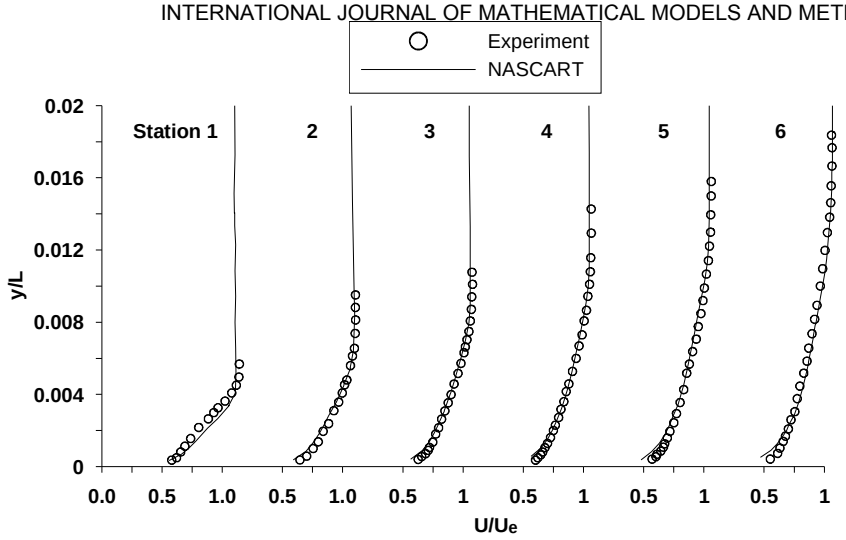

Fig. 10. Comparison of mean velocity profiles in flow field around hemispheroid.

REFERENCES

[1] Koomullil, R.P, Soni, B.K., and Singh, R.K., "A Comprehensive Generalized Mesh System for CFD Applications", *Mathematics and Computers in Simulation*, Vol. 78, Issues 5-6, 2008, pp. 605-617.

[2] Ito, Y., Shih, A. M., Erukala, A. K., Soni, B. K., Chernikov, A. N., Chrisochoides, N. P. and Nakahashi, K., "Parallel Mesh Generation Using an Advancing Front Method," *Mathematics and Computers in Simulation*, Vol. 75, Issues 5-6, 2007, pp. 200-209.

[3] DM Ingram, DM Causon and CG Mingham, "Developments in Cartesian Cut Cell Methods", *Mathematics and Computers in Simulation* 61(3-6), 2003, 561-572.

[4] Charlton, E. F., "An Octree Solution to Conservation-laws over Arbitrary Regions(OSCAE) with Applications to Aircraft Aerodynamics," Ph.D. Thesis, University of Michigan, 1997.

[5] Udaykumar, H.S., "Multiphase Dynamics in Arbitrary Geometries on Fixed Cartesian Grids," *Journal of Computational Physics*, Vol. 137, No. 2, 1997, pp. 366-405.

[6] Udaykumar, H. S., "A Sharp Interface Cartesian Grid Method for Simulating Flow with Complex Moving Boundaries," *Journal of Computational Physics*, Vol. 174, 2001, pp. 345-380.

[7] Marshall, D. D., "Extending the Functionalities of Cartesian Grid Solvers: Viscous Effects Modeling and MPI Parallelization," Ph.D. Thesis, Georgia Institute of Technology, 2002.

[8] Forrer, H., and Jeltsch, R., "A Higher Order Boundary Treatment for Cartesian-Grid Method," *Journal of Computational Physics*, Vol. 140, 1998, pp. 259-277.

[9] Dadone, A., and Grossman, B., "An Immersed Body Methodology for Inviscid Flows on Cartesian Grids," AIAA Paper 2002-1059, 2002.

[10] Launder, B. E., and Spalding, D. B., "The Numerical Computation of Turbulent Flows," *Computer Methods in Applied Mechanics and Engineering*, Vol. 3, 1974, pp. 269-289.

[11] Lee, J., "Development of an Efficient Viscous Approach in a Cartesian Grid Framework and Application to Rotor-Fuselage Interaction," Ph.D. Thesis, Georgia Institute of Technology, 2006.

[12] Hunt, D. L., and May, N. E., "Practical Use of Transport Turbulence Models in Aerospace-CFD Implementation and Applications,' AIAA Paper 99-3137, 1999.

[13] White, F. M., *Viscous Fluid Flow*, 2nd ed., McGraw-Hill, 1991.

[14] Chitsomboon, T., "Improved Artificial Viscosity for High-Reynolds-Number k-ε Turbulence Model," AIAA Paper 95-2166, 1995.

[15] Sondak, D. L., and Pletcher, R. H., "Applications of Wall Functions to Generalized Nonorthogonal Curvilinear Coordinate System," *AIAA Journal*, Vol. 33, No. 1, 1995.

[16] Nichols, R. H., and Nelson, C. C., "Wall Function Boundary Conditions Including Heat Transfer and Compressibility," *AIAA Journal*, Vol. 42, No. 6, 2004, pp. 1107-1114.

[17] Viegas, J. R., Rubesin, M. W., and Horstman, C. C., "On the Use of Wall Functions as Boundary Conditions for Two-Dimensional Separated Compressible Flow," AIAA Paper 1985-180, 1985.

[18] Holmes, D. G., and Connell, S. D., "Solution of the 2D Navier-Stokes Equations on Unstructured Adaptive Grids," AIAA Paper 89-1932-CP, 1989.

[19] Kwon, O. J., and Hah, C., "Simulation of Three-Dimensional Turbulent Flows on Unstructured Meshes," *AIAA Journal*, Vol. 33, No. 6, 1995, pp. 1081-1089.

[20] Wieghardt, K., and Tillmann, W., "On the Turbulent Friction Layer for Rising Pressure," NACA TM 1314, 1951.

[21] *Experimental Data Base for Computer Program Assessment*, AGARD Advisory Report No. 138.

[22] Abbott, I.H., and Von Doenhoff, A.E., *Theory of Wing Sections*, Dover ed., 1959.

[23] Ramaprian, B. R., Patel, V. C., and Choi, D. H., "Mean-Flow Measurements in the Three-Dimensional Boundary Layer over a Body of Revolution at Incidence," *Journal of Fluid Mechanics*, Vol. 103, 1981, pp. 479-504.